

Localized Sparsifying Preconditioner for Periodic Indefinite Systems

Fei Liu[#] and Lexing Ying^{†#}

[†] Department of Mathematics, Stanford University

[#] Institute for Computational and Mathematical Engineering, Stanford University

Abstract

This paper introduces the localized sparsifying preconditioner for the pseudospectral approximations of indefinite systems on periodic structures. The work is built on top of the recently proposed sparsifying preconditioner with two major modifications. First, the local potential information is utilized to improve the accuracy of the preconditioner. Second, an FFT based method to compute the local stencil is proposed to reduce the setup time of the algorithm. Numerical results show that the iteration number of this improved method grows only mildly as the problem size grows, which implies that solving pseudospectral approximation systems is computationally as efficient as solving sparse systems, up to a mildly growing factor.

Keywords Helmholtz equation, high frequency waves, Schrödinger equation, periodic structure, pseudospectral approximation

AMS subject classifications. 65F08, 65F50, 65N22

1 Introduction

This paper is concerned with the numerical solution of highly indefinite systems on periodic structures with periodic boundary condition

$$(-\Delta + v(x))u(x) = f(x), \quad x \in [0, 1)^d, \quad (1)$$

where d is the dimension, $f(x)$ is the right-hand side, and $u(x)$ is the unknown. $v(x)$ is the potential that can take negative values. In the case of the periodic Helmholtz equation, $v(x)$ is $-(\omega/c(x))^2$ where ω is the angular frequency and $c(x)$ is the velocity field, while for the periodic Schrödinger equation, $v(x)$ is a rescaling of $v_{\text{ext}}(x) - E$ where $v_{\text{ext}}(x)$ is the external potential field and E is the energy shift.

Solving (1) numerically is a challenging task since the system can be highly indefinite, which makes most of the classic iterative solvers no longer effective. Moreover, the solution typically has a highly oscillatory pattern and it requires large number of unknowns for accurate numerical approximations due to the Nyquist theorem.

The simplest way to solve (1) numerically is to adopt the standard second order central difference scheme, which results a sparse system, then the sparse direct methods, such as the nested dissection method [2, 1, 4], can be applied directly. However, the dispersion relation given by the standard second order central difference scheme is not accurate enough, which leads to a poor approximation

of the solution. One way to fix this is to use higher order difference schemes. The problem is that, higher order schemes require larger stencil supports, therefore the effectiveness of the sparse direct solvers cannot be leveraged.

A more natural way to discretize (1) is to use the pseudospectral method [3, 6] with Fourier basis. The pseudospectral differentiation scheme requires only a few points per oscillation of the solution to give an accurate dispersion relation. However, the stencil induced by the scheme is not local, thus the direct sparse solvers cannot be applied directly.

Recently in [7, 8], the sparsifying preconditioners are proposed to address the issue of balancing the accuracy and the sparsity pattern of the discretized systems. The main idea is to numerically convert the dense linear system derived from some accurate scheme into a sparse system and use the inverse of the sparse system as a preconditioner for the dense one. The numerical results in [8] show a satisfying iteration number for solving the Lippmann-Schwinger equation. However in [7], the iteration number needed to solve the indefinite system (1) is not as small, because the periodic boundary condition implies a higher requirement for the accuracy of the dispersion relation.

This paper is a follow-up work of [7]. We propose the localized sparsifying preconditioner which takes the local information of the potential $v(x)$ into consideration in order to give a more accurate sparse approximation of the non-sparse pseudospectral system. In addition, an FFT based method for computing the local stencils is proposed to accelerate the setup process of the preconditioner.

The rest of the paper is organized as follows. We first formulate the pseudospectral discrete system to be solved in Section 2. Section 3 briefly reviews the previous work in [7]. In Section 4 we present the modifications in this new work. Numerical results are given in Section 5. Section 6 concludes with some extra discussions.

2 Formulation of the Pseudospectral System

This section introduces the pseudospectral discretization for solving (1). Discretizing (1) with n points along each dimension results in a uniform Cartesian grid on $[0, 1)^d$, which can be indexed by the set

$$J := \{(j_1, \dots, j_d) : 0 \leq j_1, \dots, j_d < n\}.$$

The corresponding Cartesian grid is denoted by hJ where $h = 1/n$ is the step size. h is chosen such that we have at least four points per oscillation. We also introduce a grid in the Fourier domain

$$K := \{(k_1, \dots, k_d) : -n/2 \leq k_1, \dots, k_d < n/2\}.$$

Given array $z = \{z_j : j \in J\}$ defined on grid J and $\hat{z} = \{\hat{z}_k : k \in K\}$ defined on grid K , the Fourier and inverse Fourier transforms F and F^{-1} are defined as

$$\begin{aligned} \hat{z}_k &= (Fz)_k = \frac{1}{n^{d/2}} \sum_{j \in J} e^{-2\pi i(j \cdot k)/n} z_j, \quad \forall k \in K, \\ z_j &= (F^{-1}\hat{z})_j = \frac{1}{n^{d/2}} \sum_{k \in K} e^{+2\pi i(j \cdot k)/n} \hat{z}_k, \quad \forall j \in J. \end{aligned}$$

The pseudospectral method discretizes the minus Laplacian operator with

$$L := F^{-1} \text{diag}(4\pi^2 |k|^2)_{k \in K} F$$

which results in the discretized equation of (1)

$$(L + \text{diag}(v))u = f, \quad (2)$$

where, for example, $f = \{f_j = f(hj) : j \in J\}$ and $v = \{v_j = v(hj) : j \in J\}$ are the discrete arrays generated from sampling the values of $f(x)$ and $v(x)$ on the grid hJ , respectively. $u = \{u_j : j \in J\}$ is the numerical solution on hJ , where u_j stands for an approximation of $u(hj)$. In what follows, we will use lower case letters to denote discrete arrays on grids J and K , which should not cause any ambiguity.

3 Brief Review of the Sparsifying Preconditioner

In this section we use a simplified version of the sparsifying preconditioner in [7] to review the main idea. While Equation (2) gives an accurate dispersion relation, the numerical stencil is not local, which makes the sparse direct methods no longer applicable. The sparsifying preconditioner addresses this issue by approximating (2) with a carefully designed sparse system, as we shall see in what follows.

Define $s := (1/|J|) \sum_{j \in J} v_j$ as the average of v (a scalar that is often quite negative in interesting cases, $s \sim O(n^2)$) and $q := v - s$ as the zero-mean shift of v . Then (2) can be rewritten as

$$(L + s + \text{diag}(q))u = f. \quad (3)$$

The reason why we want q to have zero-mean will be explained below.

We assume without loss of generality that $(L + s)$ is invertible, otherwise we perturb s by a small shift. The inverse of $(L + s)$, which is a highly indefinite matrix, is given by

$$G := (L + s)^{-1} = F^{-1} \text{diag} \left(\frac{1}{4\pi^2 |k|^2 + s} \right)_{k \in K} F,$$

which can be applied efficiently using FFT. Applying G to both sides of (3) gives

$$(I + G \text{diag}(q))u = Gf := g. \quad (4)$$

The main motivation of the sparsifying preconditioner is that, G is a Green's matrix induced from a partial differential equation and the operators in the equation are local. Suppose the step size h is small enough, then if we discretize the equation with standard second order central difference scheme and we denote the resulting discrete operator as A , which is a sparse matrix, we will have that $AG \approx I$. Though the central difference scheme is not accurate enough when we only have a small number of points per oscillation, it is still reasonable to seek for some sparse matrix Q as a "sparse discretization" of the equation, such that QG is also sparse approximately, and by applying Q on both sides of (4) we get an approximately sparse system. The main task now is to find a Q such that

1. Q is sparse and local,
2. QG is approximately sparse and local.

Here, by “sparse and local”, we mean that the non-zero elements in row j only involve the nearby neighbors of j . If we could find such a Q and denote $C \approx QG$ as the sparse approximation, then applying Q to (4) gives

$$(Q + QG \operatorname{diag}(q))u = Qg, \quad (5)$$

which can be approximated by the sparse system

$$(Q + C \operatorname{diag}(q))\tilde{u} = Qg, \quad (6)$$

where \tilde{u} stands for an approximation of u . The sparse matrix $(Q + C \operatorname{diag}(q))$ can be inverted by the nested dissection algorithm which gives rise to an efficient preconditioner $(Q + C \operatorname{diag}(q))^{-1}Q$ to solve (4).

To find such Q , we introduce the notation of neighborhood μ_j for each $j \in J$

$$\mu_j := \{i : \|i - j\|_\infty \leq 1\},$$

which is the set containing j and its nearest neighbors in l_∞ norm. Then the requirements for Q can be formulated as

1. $Q[j, \mu_j^c] = 0$,
2. $(QG)[j, \mu_j^c] = Q[j, :]G[:, \mu_j^c] = Q[j, \mu_j]G[\mu_j, \mu_j^c] \approx 0$,

where the notation $[\cdot, \cdot]$ means the submatrix of certain rows and columns. For example, $Q[j, \mu_j^c]$ is the submatrix of Q restricted to row j and columns in μ_j^c . The superscript c stands for complement and $\mu_j^c = J \setminus \mu_j$.

To find a proper choice for $Q[j, \mu_j]$, we consider the following optimization problem:

$$\min_{\|\alpha\|_2=1} \|\alpha^T G[\mu_j, \mu_j^c]\|_2,$$

where $\alpha \in \mathbb{R}^{|\mu_j| \times 1}$ is a column vector. Let $G[\mu_j, \mu_j^c] = U\Sigma V^T$ be the singular value decomposition. Then the optimal solution for α is given by

$$\alpha := U[:, |\mu_j|],$$

where $|\cdot|$ means cardinality and α is the left singular vector corresponding to the smallest singular value. We set

$$Q[j, \mu_j] := \alpha^T,$$

then $\|(QG)[j, \mu_j^c]\|_2$ is minimized and the optimal value is the smallest singular value. We expect the smallest singular value to be small because the partial differential equation itself implies that there should exist some local discretization to cancel the off diagonal elements of the Green's matrix approximately.

Once Q is ready, we set C as the truncation of QG by

$$\begin{aligned} C[j, \mu_j] &:= Q[j, \mu_j]G[\mu_j, \mu_j], \\ C[j, \mu_j^c] &:= 0. \end{aligned}$$

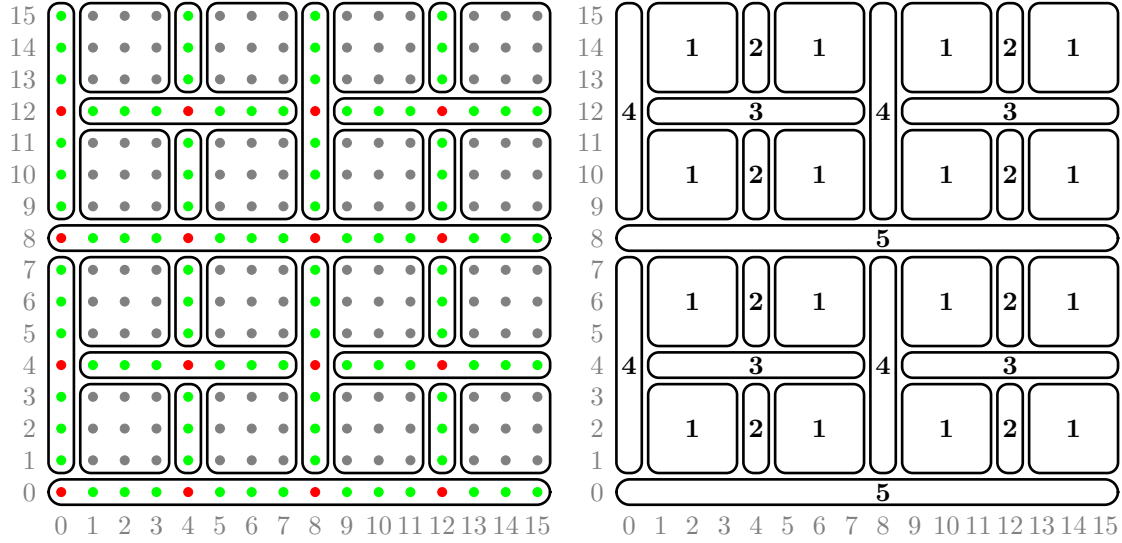


Figure 1: This figure shows a 16×16 example of the nested dissection algorithm. Left: The unknowns are grouped hierarchically. The gray points are the box-points in the nested dissection algorithm, the green ones are the edge-points and the red ones are the vertex-points. Right: the hierarchical elimination order is shown for each group. We first eliminate the box points **1** to their boundary neighbors and then eliminate the boundary points **2** to their remaining neighbors and so on so forth.

As a result, the matrix $P := Q + C \text{diag}(q)$ has the same sparsity pattern as Q . By exploiting this sparsity, one can apply the nested dissection algorithm which reorders the unknowns hierarchically to minimize the elimination cost to solve the sparse system (6). Figure 1 gives an example of the nested dissection algorithm in 2D.

We would like to point out that α , $Q[j, \mu_j]$ and $C[j, \mu_j]$ do not depend on j due to the translational invariance of G . Hence one only needs to perform the SVD and calculate the stencils $Q[j, \mu_j]$ and $C[j, \mu_j]$ just once.

4 Localized Sparsifying Preconditioner

This section introduces the localized sparsifying preconditioner, which is based on the sparsifying preconditioner in the previous section but with two major improvements discussed below.

4.1 Using the local potential information

In Section 3, the scalar shift s is chosen to be the average of v such that q has a zero-mean. The reason for choosing s to be the average is that, the error introduced in (6) comes from the truncation of QG . The truncated part, which should have been multiplied by the elements in q , is neglected in (6), and if q is small in magnitude, then the error introduced is expected to be small. The algorithm chooses s such that q has a zero-mean to make the residual relatively small with a single

shift. However, it does not eliminate all the errors. When $v(x)$ has large variations, the residual array q could still be large.

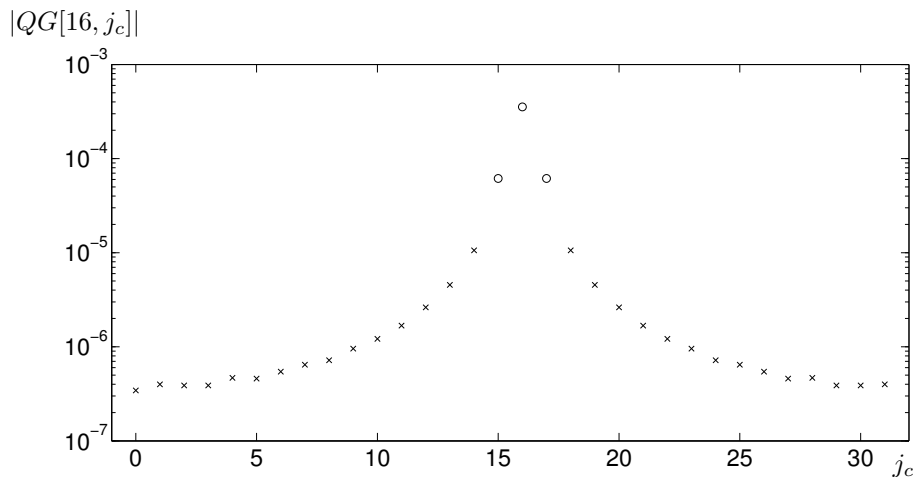


Figure 2: This figure shows the magnitude of the j -th row of QG in logarithmic scale, where $n = 32, j = 16$, and the shift $s = -62\pi^2$. The x-axis is the column index j_c ranging from 0 to 31 and the y-axis is $|QG[16, j_c]|$. The entries with marks “o” are reserved and the ones with “x” are truncated. We can see the decay of the truncated entries as j_c gets far away from the center position $j = 16$.

Taking a closer look at the j -th row of QG , we find that the truncated elements tend to be big near j . Figure 2 shows a row of QG in the 1D case, which indicates a decaying trend of the elements of the j -th row of QG when the column index gets far away from j . It tells us that, if we choose the shift s such that q is small near j , then the truncated elements in the j -th row of $QG \text{diag}(q)$ will be more likely to be diminished, since the dominating elements in QG are multiplied with small elements in q . This suggests that, it is helpful to set the shift s to be close to v_j to reduce the error introduced by truncating the j -th row of $QG \text{diag}(q)$. Ideally, it would be nice if, for each j , one could use the Green’s matrix $G_{v_j} := (L + v_j)^{-1}$ to compute the SVD and set the stencils by

$$\begin{aligned} G_{v_j}[\boldsymbol{\mu}_j, \boldsymbol{\mu}_j^c] &= U \Sigma V^T, \\ \alpha_{v_j} &:= U[:, |\boldsymbol{\mu}_j|], \\ Q[j, \boldsymbol{\mu}_j] &:= \alpha_{v_j}^T, \\ C[j, \boldsymbol{\mu}_j] &:= Q[j, \boldsymbol{\mu}_j] G_{v_j}[\boldsymbol{\mu}_j, \boldsymbol{\mu}_j], \end{aligned}$$

in which case the truncated part tends to be much smaller.

However, computing each row of Q and C with a unique shift is expensive. To save computational cost, a list of possible shifts is created in advance. Then our method only computes the local stencils corresponding to the shifts in the list and assigns the stencil at position j to the shift closest to v_j . More specifically, we first choose a set S which contains a list of shifts s distributed evenly in the range of v . The method of choosing S will be discussed later. Then for each $s \in S$, one computes

α_s by

$$\begin{aligned} G_s &:= (L + s)^{-1}, \\ G_s[\boldsymbol{\mu}_j, \boldsymbol{\mu}_j^c] &= U \Sigma V^T, \\ \alpha_s &:= U[:, |\boldsymbol{\mu}_j|]. \end{aligned}$$

Notice that the value of α_s does not depend on j due to the translational invariant property of G_s .

After calculating α_s for each s , our method sets a shift s_j for each j to be the shift s closest to v_j in S

$$s_j := \min\{|s - v_j| : s \in S\},$$

which means s_j serves as an approximation of the local shift v_j hence it is location dependent. However, the singular vector α_{s_j} only needs to be computed once for different locations sharing the same shift approximation. Thus the number of Green's matrices and SVDs that need to be formed only depends on the range of the potential shift v , not on the number of discrete points. That saves us the computational cost, especially in 3D case.

With α_{s_j} , one computes the following stencils for each j

$$\begin{aligned} Q[j, \boldsymbol{\mu}_j] &:= \alpha_{s_j}^T, \\ C[j, \boldsymbol{\mu}_j] &:= Q[j, \boldsymbol{\mu}_j] G_{s_j}[\boldsymbol{\mu}_j, \boldsymbol{\mu}_j], \\ P[j, \boldsymbol{\mu}_j] &:= Q[j, \boldsymbol{\mu}_j] + C[j, \boldsymbol{\mu}_j] \text{diag}(v[\boldsymbol{\mu}_j] - s_j) \end{aligned}$$

where $v[\boldsymbol{\mu}_j]$ is the array v restricted to $\boldsymbol{\mu}_j$. Now multiplying G_{s_j} to (2) on both sides gives

$$(I + G_{s_j} \text{diag}(v - s_j))u = G_{s_j} f. \quad (7)$$

Next multiplying by $Q[j, \boldsymbol{\mu}_j]$ to the rows indexed by $\boldsymbol{\mu}_j$ in (7) and truncating the elements not in $\boldsymbol{\mu}_j$ gives rise to

$$P[j, \boldsymbol{\mu}_j]u[\boldsymbol{\mu}_j] \approx C[j, \boldsymbol{\mu}_j]f[\boldsymbol{\mu}_j].$$

Assembling all the approximating equations for different positions j results in the following equation

$$P\tilde{u} = Cf, \quad (8)$$

where \tilde{u} serves as an approximation of u . By applying the nested dissection algorithm, one can use $P^{-1}C$ as an efficient preconditioner for (2). We see that the local potential information is taken into consideration to build the preconditioner, which is the main advantage of this new approach.

Now let us discuss how to choose S . Denote v_{\min} and v_{\max} as the minimum and maximum value of v respectively. To approximate all local potential values in the interval $[v_{\min}, v_{\max}]$ by a minimal distance, our method distributes the shifts in S evenly in $[v_{\min}, v_{\max}]$. Another important point for choosing the shift s is to avoid resonance, which means, we do not want $(L + s)$ to be singular. A simple way to avoid resonance is to choose s to have the form $(4m + 2)\pi^2$ where $m \in \mathbb{Z}$, since the eigenvalues of L are all multiples of $4\pi^2$. For the size of the shift list S , the numerical tests in Section 5 show that it suffices to set $|S| = O(n)$ to get an ideal iteration number.

4.2 Computing local stencils using FFT

As pointed out in [7], building compact stencils that only involve the nearest neighbors fails to give a preconditioner accurate enough. [7] solves this issue by treating the points in the same leaf box of the nested dissection algorithm as a whole and increasing the size of the leaf box as the problems size grows. This paper adopts a different approach.

For each $s \in S$, we not only build the stencil involving the nearest neighbors but also the ones involving neighbors at a larger distance, in order to get more accurate local schemes. Then, for each position j , our method picks the most accurate stencil that involves the largest possible neighborhood such that the nested dissection algorithm can still be applied. More specifically, define

$$\mu_j^t := \{i : \|i - j\|_\infty \leq t\}$$

where t controls the size of the neighborhood and t is typically set to be bounded by 4. For example, $t = 1$ corresponds to the compact stencil we discussed above. For each (s, t) pair, we compute

$$\begin{aligned} G_s[\mu_j^t, (\mu_j^t)^c] &= U \Sigma V^T, \\ \alpha_s^t &:= U[:, |\mu_j^t|], \end{aligned}$$

where α_s^t does not depend on j due to the translational invariance of the Green's matrix, and we can simply use $G_s[\mu_0^t, (\mu_0^t)^c]$ to compute the SVD.

Now for each j , set $s = s_j$ and choose t as big as possible such that the sparsity pattern requirement for the nested dissection algorithm is satisfied. Figure 3 shows an example for the choice of t for different points, where a point nearer to the center of a box has a larger t value. In what follows, we denote t_j as this neighbor size chosen for the position j . Then the stencils are given by

$$\begin{aligned} Q[j, \mu_j^{t_j}] &:= (\alpha_{s_j}^{t_j})^T, \\ C[j, \mu_j^{t_j}] &:= Q[j, \mu_j^{t_j}] G_{s_j}[\mu_j^{t_j}, \mu_j^{t_j}], \\ P[j, \mu_j^{t_j}] &:= Q[j, \mu_j^{t_j}] + C[j, \mu_j^{t_j}] \text{diag}(v[\mu_j^{t_j}] - s_j), \end{aligned}$$

where $v[\mu_j^{t_j}]$ stands for restricting the vector v to the index set $\mu_j^{t_j}$.

Let us discuss the computational cost of building the stencils. First, the cost of forming the Green's matrix G_s is $O(N \log N)$ since we only need to compute a single column of G_s via FFT. Next, if we use the SVD of $G_s[\mu_0^t, (\mu_0^t)^c]$ directly to compute α_s^t , the cost will be $O(t^{2d}N)$, which can dominate the $O(N \log N)$ complexity in practice even when t is as small as 2 or 3. To reduce the cost, consider the following identity

$$G_s[\mu_0^t, (\mu_0^t)^c] G_s[\mu_0^t, (\mu_0^t)^c]^T = G_s[\mu_0^t, :] G_s[\mu_0^t, :]^T - G_s[\mu_0^t, \mu_0^t] G_s[\mu_0^t, \mu_0^t]^T \quad (9)$$

$$:= A_1 - A_2. \quad (10)$$

In order to compute α_s^t , one only needs to calculate the eigenvalue decomposition of $(A_1 - A_2)$ and extract the eigenvector corresponding to the smallest eigenvalue. A nice property of (10) is that, the elements in A_1 are dot products of the rows of G_s , which are essentially the values of the convolution of the kernel vector with itself. To explain in details, denote g_s as the kernel vector of G_s with periodic extension over Z^d . Then

$$\begin{aligned} G_s[j_1, j_2] &= g_s[j_1 - j_2], \quad \forall j_1, j_2 \in J, \\ g_s[j] &= g_s[-j], \quad \forall j \in J. \end{aligned}$$

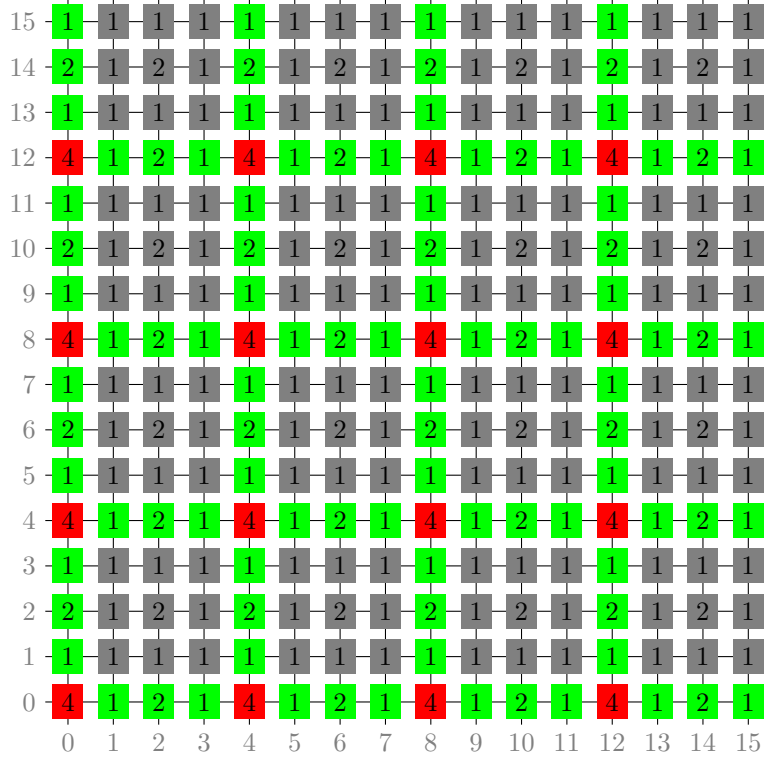


Figure 3: This figure shows a 16×16 example of the choice of t in 2D. The gray points are the box-points in the nested dissection algorithm, the green ones are the edge-points and the red ones are the vertex-points. The maximum choice of t is marked out for each point. To satisfy the sparsity pattern requirement for the nested dissection algorithm, the interaction between two points cannot cross edges. For example, two box-points in different boxes cannot interact with each other. We see that for the box-points, the ones nearer to the box center have larger stencil supports. We also note that the vertex-points can have larger supports without breaking the sparsity requirement.

The entries in A_1 have the form $G_s[j_1, :]G_s[j_2, :]^T$, which can be written as

$$\begin{aligned}
 G_s[j_1, :]G_s[j_2, :]^T &= \sum_{j \in J} g_s[j_1 - j]g_s[j - j_2] \\
 &= \sum_{j \in J} g_s[j_1 - j_2 - j]g_s[j] \\
 &= (g_s * g_s)[j_1 - j_2].
 \end{aligned}$$

The convolution $g_s * g_s$ can be computed by FFT in $O(N \log N)$ steps. After computing the convolution, retrieving the entries in A_1 costs only $O(t^{2d})$ steps. Retrieving the other entries in (10) and computing the eigenvalue decomposition take $O(t^{3d})$ steps so the total cost is $O(N \log N + t^{3d})$ for computing the stencil α_s^t for each (s, t) pair. Here $O(t^{3d})$ is negligible compared to $O(N \log N)$ in practical cases. In addition, the computation of the convolution of g_s with itself only needs to be

performed once for different t values, so there is only little extra cost for building stencils involving larger range of neighbor points. The overall computational costs are listed in Table 1.

	T_{stencil}	T_{NDsetup}	T_{NDapp}
2D	$O(S (N \log N + t^6))$	$O(N^{3/2} + b^4 N)$	$O(N \log N + b^2 N)$
3D	$O(S (N \log N + t^9))$	$O(N^2 + b^6 N)$	$O(N^{4/3} + b^3 N)$

Table 1: The time costs of the algorithm. T_{stencil} is the cost of computing the stencils used for building Q, C and P . T_{NDsetup} is the setup cost of the nested dissection algorithm and T_{NDapp} is the application cost per iteration. $N = n^d$ is the degree of freedom. b is the size of the leaf box in the nested dissection algorithm. t is the size of the largest neighborhood and $|S|$ is the size of the shift list.

5 Numerical Results

This section presents the numerical results for the Helmholtz equation and the Schrödinger equation in 2D and 3D. The algorithm is implemented in MATLAB and the tests are performed on a server with four Intel Xeon E5-4640 CPUs and a max usage of 384 GB memory. The preconditioner is combined with standard GMRES solver with relative tolerance 10^{-6} and restart value 40. The notations in the numerical tests are listed as follows.

- ω is the angular frequency.
- $N = n^d$ is the number of unknowns.
- $|S|$ is the size of the shift list.
- T_{stencil} is the time cost of computing the stencils in seconds.
- T_{NDsetup} is the setup cost of the nested dissection algorithm in seconds.
- N_{iter} is the iteration number.
- T_{NDsolve} is the solve cost of the nested dissection algorithm in seconds.

Our method computes the stencils for $t = 1, 2$ and sets $|S| = O(n)$. The leaf box in the nested dissection algorithm b is fixed to be 8. The right-hand side for each test is a Gaussian point source at the center of the domain.

Helmholtz Equation. For the Helmholtz equation, $v(x) = -(\omega/c(x))^2$ where ω is the angular frequency and $c(x)$ is the velocity field. Two velocity fields in 2D are tested:

- (i). A constant background with a Gaussian profile in the center of the square.
- (ii). A constant background with a cross shape profile.

The results are given in Tables 2 and 3.

Two similar tests are performed in 3D, where the velocity fields are

$\omega/(2\pi)$	N	$ S $	T_{stencil}	T_{NDsetup}	N_{iter}	T_{NDsolve}
16	64^2	4	$1.89e-02$	$5.25e-02$	6	$4.00e-02$
32	128^2	8	$2.71e-02$	$2.27e-01$	5	$1.39e-01$
64	256^2	16	$8.30e-02$	$8.91e-01$	6	$6.74e-01$
128	512^2	32	$3.87e-01$	$4.23e+00$	6	$2.56e+00$

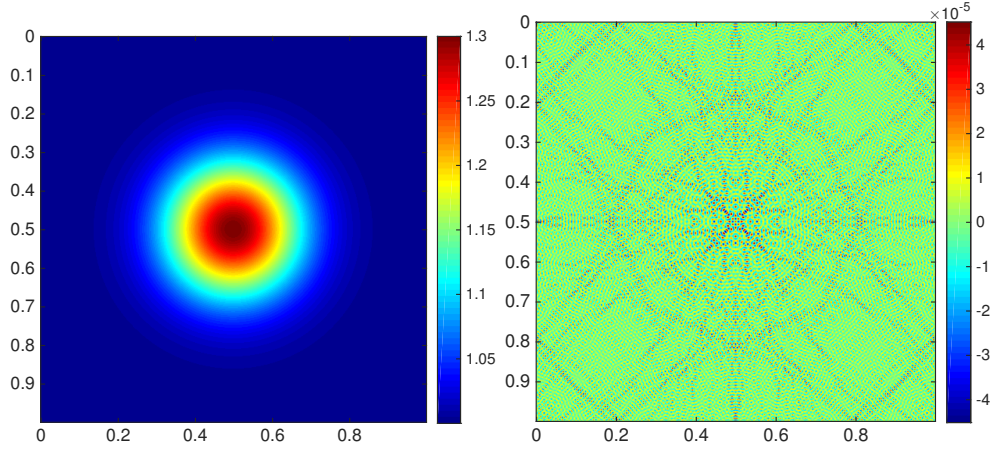


Table 2: Results for velocity field (i) of the 2D Helmholtz equation. Top: numerical results. Bottom: $c(x)$ (left) and $u(x)$ (right) for the largest problem size.

- (i). A constant background with a Gaussian profile in the center of the cube.
- (ii). A constant background with a cross shape profile, where three cylinders cross the domain along the three axes correspondingly.

The results are summarized in Tables 4 and 5.

From the numerical tests for the Helmholtz equation one can make the following two observations:

1. The iteration numbers are not sensitive to the growth of the problem size. In almost all cases, the preconditioned iterative solver converges in about 6-7 iterations. This clearly shows significant improvement over the results reported in [7].
2. The construction cost of the stencils is dominated by the setup cost of the nested dissection algorithm. This domination is more noteworthy in 3D due to a larger scaling difference between the stencil construction cost and the setup cost of the nested dissection factorization.

Schrödinger Equation. For the Schrödinger equation, we set the system size to be $n = 1/h$. With the right rescaling, $v(x) = v_{\text{ext}}(x/h)/h^2 - E/h^2$ where $v_{\text{ext}}(x)$ is the external potential field and E is the energy shift. We set $E = 2.4$ so that there are at least four points per oscillation. The potential fields tested for 2D are

- (i). An array of randomly put 2D Gaussians in the square.
- (ii). An equal spaced array of 2D Gaussians with one missing at the center of the square.

$\omega/(2\pi)$	N	$ S $	T_{stencil}	T_{NDsetup}	N_{iter}	T_{NDsolve}
16	64^2	4	$8.39e-03$	$5.23e-02$	6	$3.66e-02$
32	128^2	8	$3.89e-02$	$2.12e-01$	6	$1.66e-01$
64	256^2	16	$7.66e-02$	$9.10e-01$	6	$6.67e-01$
128	512^2	32	$3.62e-01$	$4.49e+00$	5	$2.51e+00$

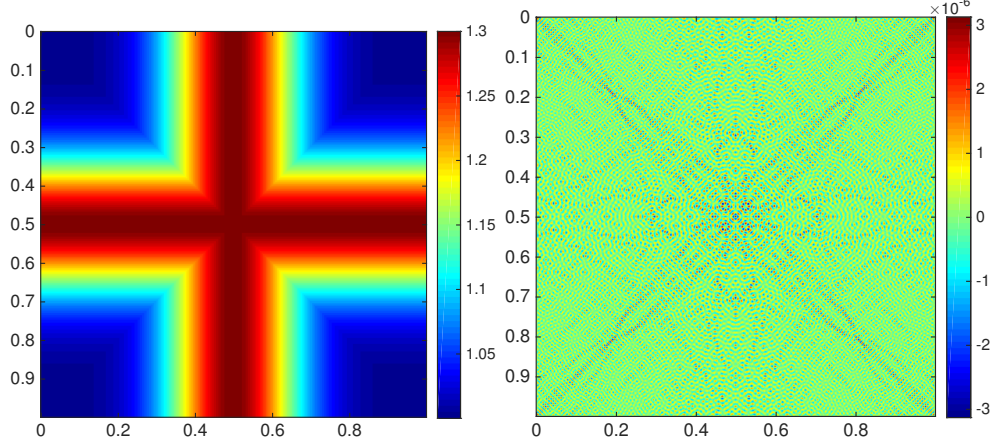


Table 3: Results for velocity field (ii) of the 2D Helmholtz equation. Top: numerical results. Bottom: $c(x)$ (left) and $u(x)$ (right) for the largest problem size.

$\omega/(2\pi)$	N	$ S $	T_{stencil}	T_{NDsetup}	N_{iter}	T_{NDsolve}
4	16^3	4	$4.80e-02$	$2.55e-01$	6	$8.55e-02$
8	32^3	8	$8.37e-02$	$6.20e+00$	6	$9.10e-01$
16	64^3	16	$3.73e-01$	$1.70e+02$	6	$1.20e+01$
32	128^3	32	$3.53e+00$	$8.72e+03$	9	$2.07e+02$

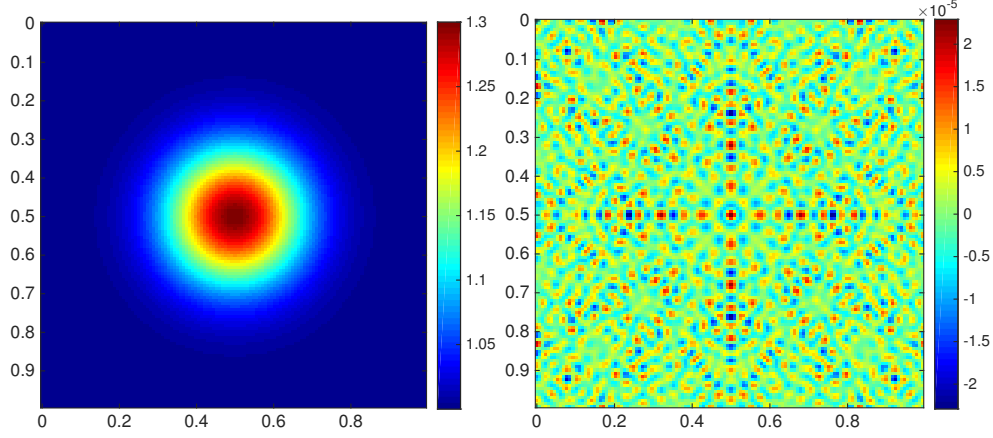


Table 4: Results for velocity field (i) of the 3D Helmholtz equation. Top: numerical results. Bottom: $c(x)$ (left) and $u(x)$ (right) at $x_3 = 0.5$ for the largest problem size.

$\omega/(2\pi)$	N	$ S $	T_{stencil}	T_{NDsetup}	N_{iter}	T_{NDsolve}
4	16^3	4	$3.76e-02$	$2.91e-01$	7	$9.51e-02$
8	32^3	8	$8.60e-02$	$6.00e+00$	6	$9.93e-01$
16	64^3	16	$3.85e-01$	$1.64e+02$	6	$1.12e+01$
32	128^3	32	$4.07e+00$	$8.64e+03$	7	$1.47e+02$

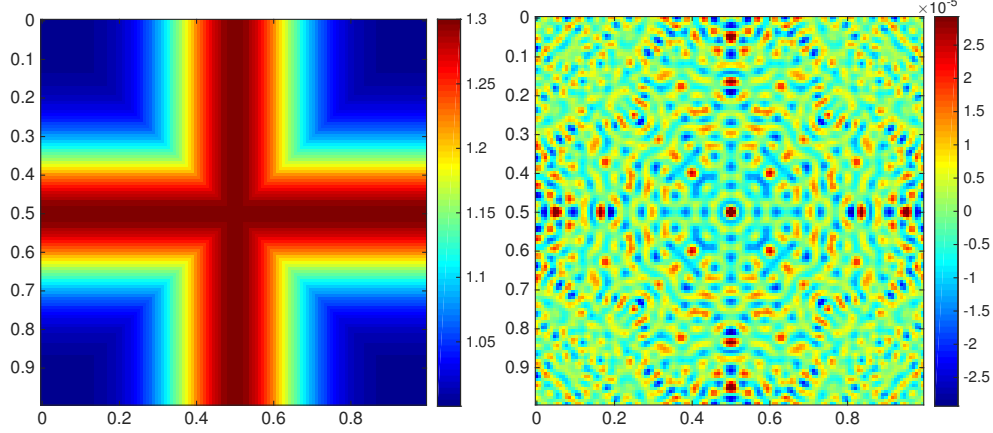


Table 5: Results for velocity field (ii) of the 3D Helmholtz equation. Top: numerical results. Bottom: $c(x)$ (left) and $u(x)$ (right) at $x_3 = 0.5$ for the largest problem size.

The results are given in Tables 6 and 7.

For 3D tests, the potential fields are

- (i). An array of randomly put 3D Gaussians in the cube.
- (ii). An equal spaced array of 3D Gaussians with one missing at the center of the cube.

The results are shown in Tables 8 and 9.

For the Schrödinger equation, the iteration number grows slightly faster. The reason is that the variation of the field $v(x)$ increases as the problem size increases in the Schrödinger equation case, while for the Helmholtz equation only ω grows with the problem size and $c(x)$ remains the same. Thus the tests for the Schrödinger equation are more challenging due to larger local variations of the potential field. Nevertheless, the growths of the iteration numbers in the tests of the Schrödinger equation are still mild compared to the growth of the problem size.

6 Conclusion

This paper introduces the localized sparsifying preconditioner for the pseudospectral approximations of indefinite systems on periodic structures based on the preconditioners in [7, 8]. The novelty includes two parts. First, the local potential information is taken into consideration during the construction of the sparse matrices, which lowers the iteration number. Second, an FFT based approach is introduced to compute the stencil which improves the efficiency of the setup process of the algorithm.

N	$ S $	T_{stencil}	T_{NDsetup}	N_{iter}	T_{NDsolve}
64^2	4	$2.11e-02$	$5.89e-02$	7	$5.58e-02$
128^2	8	$3.66e-02$	$2.28e-01$	8	$2.28e-01$
256^2	16	$9.70e-02$	$9.76e-01$	8	$8.80e-01$
512^2	32	$3.83e-01$	$4.28e+00$	10	$4.18e+00$

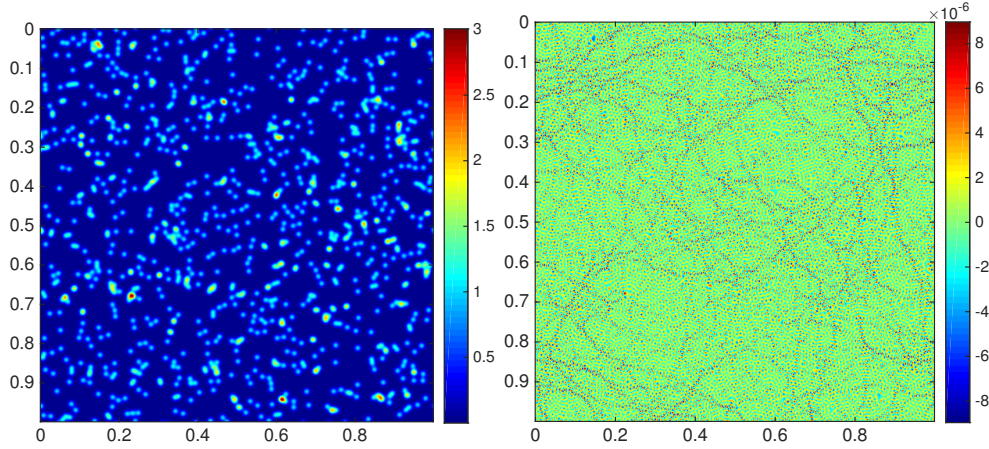


Table 6: Results for potential field (i) of the 2D Schrödinger equation. Top: numerical results. Bottom: $v_{\text{ext}}(x/h)$ (left) and $u(x)$ (right) for the largest problem size.

Numerical tests show that the iteration number grows only mildly when the problem size increases, which implies that solving pseudospectral approximations of indefinite systems on periodic structures is not inherently harder than solving sparse systems, up to a mildly growing factor.

Another advantage of this new preconditioner is that, the construction of the stencils of the algorithm is independent of the setup stage of the nested dissection algorithm. The potential shift list S needs little information about the actual potential field $v(x)$ except for the minimum and the maximum value, which means that the stencils can be built in advance, and as long as the value of $v(x)$ is in a certain range, there is no need to reconstruct the stencil no matter how $v(x)$ varies. This can be helpful when an iterative process is involved or $v(x)$ is constantly changing, such as in [5].

The choice of t for each location in the current setting is rather crude. There are several ways to make potential improvements. For example, one can adopt the stencil where $t = 1$ only for the largest skeleton in the nested dissection algorithm, while for the rest of the points, stencils with higher t values can be used. In this way, the setup cost of the nested dissection algorithm will not increase too much, while the iteration number may be further reduced. One can also use the stencils with lower t values for the locations where the local potential field variation is milder and with higher t values where the variation is more drastic. These techniques can be helpful for practical application of this algorithm.

N	$ S $	T_{stencil}	T_{NDsetup}	N_{iter}	T_{NDsolve}
64^2	4	$1.89e-02$	$5.35e-02$	6	$4.46e-02$
128^2	8	$3.06e-02$	$2.32e-01$	7	$2.12e-01$
256^2	16	$9.47e-02$	$8.59e-01$	7	$7.89e-01$
512^2	32	$3.46e-01$	$4.23e+00$	9	$3.69e+00$

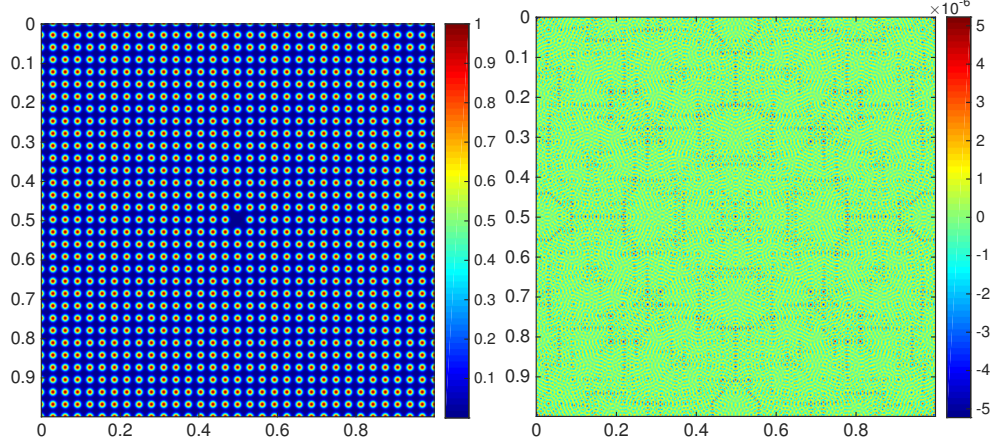


Table 7: Results for potential field (ii) of the 2D Schrödinger equation. Top: numerical results. Bottom: $v_{\text{ext}}(x/h)$ (left) and $u(x)$ (right) for the largest problem size.

N	$ S $	T_{stencil}	T_{NDsetup}	N_{iter}	T_{NDsolve}
16^3	4	$3.53e-02$	$2.58e-01$	7	$7.53e-02$
32^3	8	$8.70e-02$	$6.16e+00$	12	$1.86e+00$
64^3	16	$3.99e-01$	$1.68e+02$	9	$1.57e+01$
128^3	32	$3.33e+00$	$8.65e+03$	10	$2.19e+02$

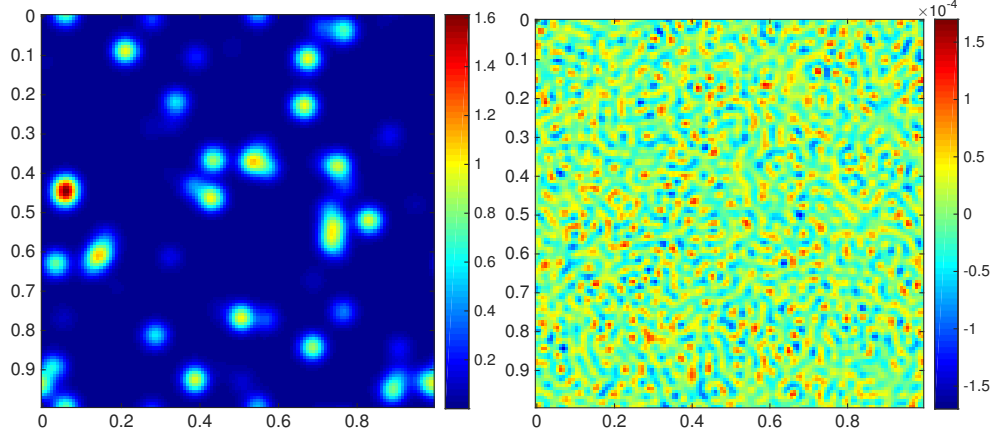


Table 8: Results for potential field (i) of the 3D Schrödinger equation. Top: numerical results. Bottom: $v_{\text{ext}}(x/h)$ (left) and $u(x)$ (right) at $x_3 = 0.5$ for the largest problem size.

N	$ S $	T_{stencil}	T_{NDsetup}	N_{iter}	T_{NDsolve}
16^3	4	$3.16e-02$	$2.85e-01$	6	$7.16e-02$
32^3	8	$1.08e-01$	$6.14e+00$	7	$1.06e+00$
64^3	16	$3.99e-01$	$1.66e+02$	7	$1.32e+01$
128^3	32	$3.61e+00$	$8.54e+03$	7	$1.48e+02$

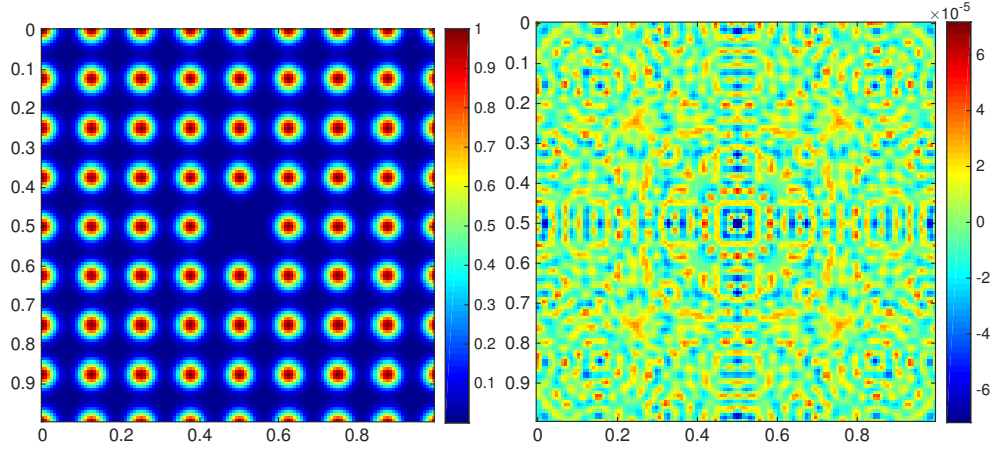


Table 9: Results for potential field (ii) of the 3D Schrödinger equation. Top: numerical results. Bottom: $v_{\text{ext}}(x/h)$ (left) and $u(x)$ (right) at $x_3 = 0.5$ for the largest problem size.

Acknowledgments

The authors are partially supported by the National Science Foundation under award DMS-1521830 and the U.S. Department of Energy’s Advanced Scientific Computing Research program under award DE-FC02-13ER26134/DE-SC0009409.

References

- [1] I. S. Duff and J. K. Reid. The multifrontal solution of indefinite sparse symmetric linear equations. *ACM Trans. Math. Software*, 9(3):302–325, 1983.
- [2] A. George. Nested dissection of a regular finite element mesh. *SIAM J. Numer. Anal.*, 10:345–363, 1973. Collection of articles dedicated to the memory of George E. Forsythe.
- [3] D. Gottlieb and S. A. Orszag. *Numerical analysis of spectral methods: theory and applications*. Society for Industrial and Applied Mathematics, Philadelphia, Pa., 1977. CBMS-NSF Regional Conference Series in Applied Mathematics, No. 26.
- [4] J. W. H. Liu. The multifrontal method for sparse matrix solution: theory and practice. *SIAM Rev.*, 34(1):82–109, 1992.
- [5] J. Lu and L. Ying. Sparsifying preconditioner for soliton calculations. *J. Comput. Phys.*, 315(C):458–466, June 2016.

- [6] L. N. Trefethen. *Spectral methods in MATLAB*, volume 10 of *Software, Environments, and Tools*. Society for Industrial and Applied Mathematics (SIAM), Philadelphia, PA, 2000.
- [7] L. Ying. Sparsifying preconditioner for pseudospectral approximations of indefinite systems on periodic structures. *Multiscale Model. Simul.*, 13(2):459–471, 2015.
- [8] L. Ying. Sparsifying preconditioner for the Lippmann-Schwinger equation. *Multiscale Model. Simul.*, 13(2):644–660, 2015.